

Interplay between quantum confinement and dielectric mismatch for ultra-shallow dopants.

J.A. Mol,^{1,2} J. Salfi,¹ J.A. Miwa,¹ M.Y. Simmons,¹ and S. Rogge^{1,2}

¹*Centre for Quantum Computation and Communication Technology,
University of New South Wales, Sydney NSW 2052, Australia*

²*Kavli Institute of Nanoscience, Delft University of Technology, Lorentzweg 1, 2628 CJ Delft, The Netherlands*
(Dated: March 13, 2013)

Understanding the electronic properties of dopants near an interface is a critical challenge for nano-scale devices. We have determined the effect of dielectric mismatch and quantum confinement on the ionization energy of individual acceptors beneath a hydrogen passivated silicon (100) surface. Whilst dielectric mismatch between the vacuum and the silicon at the interface results in an image charge which enhances the binding energy of sub-surface acceptors, quantum confinement is shown to reduce the binding energy. Using scanning tunneling spectroscopy we measure resonant transport through the localized states of individual acceptors. Thermal broadening of the conductance peaks provides a direct measure for the absolute energy scale. Our data unambiguously demonstrates that these two independent effects compete with the result that the ionization energy is less than 5 meV lower than the bulk value for acceptors less than a Bohr radius from the interface.

The operation of semiconductor devices is based on the possibility to locally change the electron properties of the host material by means of doping. As device dimensions continue to decrease, the surface-to-volume ratio of active channels increases and the effect of the semiconductor-insulator interface on local doping starts to dominate device properties [1]. Previous studies have suggested that dielectric mismatch at the semiconductor-insulator interface leads to an increase in ionization energy of dopants near the interface [2, 3]. In silicon nanowires this leads to doping deactivation and consequently an increase of resistivity with decreasing diameter [2, 4]. However, recent transport spectroscopy experiments on single arsenic donors in gated nanowires did not report an appreciable increase in ionization energy [5]. These results appear contradictory.

The ionization energies of shallow donor and acceptor impurities are qualitatively described by effective mass theory [6], which works especially well for light impurity atoms such as Li and B. Since the Coulomb potential is strongly screened due to the polarization of the semiconductor, the ionization energy of dopant impurities is only in the order of tens of meV. This simple picture breaks down in the presence of an interface. Dielectric mismatch between the semiconductor material and its surroundings is predicted to enhance the ionization energy [4]. Moreover, for nanowires it is well known that when the thickness of the nanowire approaches the Bohr radius of the impurity the ionization energy *increases* due to quantum confinement [7, 8]. However, in the case of a half-space, i.e. a flat interface, effective mass theory predicts a *decrease* in the ionization energy due to quantum confinement [9, 10]. As a result of these two competing effects, dielectric mismatch and quantum confinement, the ionization energy of dopant near a flat interface is expected to be bulk-like [9, 10].

Here, we use low-temperature (4.2 K) scanning

tunneling spectroscopy (STS) to directly measure the ionization energy of boron acceptors beneath the hydrogen terminated Si(100) surface ($N_A \sim 8 \times 10^{18} \text{ cm}^{-3}$). Previous studies on GaAs(110) [11–15], InAs(110) [16] and ZnO(0001) [17] surfaces have proven that STS is a powerful tool to study sub-surface impurities. Using scanning tunneling microscopy the surroundings of each individual dopant atom can be imaged and therefore any effect of dopant clustering or interface disorder, such as charge traps, on the ionization energy of the acceptors may be excluded. By analyzing the line shape of differential conductance within well known single electron spectroscopy formalisms, we conclude that transport is thermally broadened. Consequently, we can use the electron temperature of the sample as a reference to calibrate the coupling between the applied bias voltage and the potential landscape at the semiconductor-vacuum interface. In such a way we are able to obtain a direct measure for the acceptor ionization energy. Moreover, STS allows us to determine the distance of individual acceptors to the interface by measuring the spectral shift of the valence band due to the negatively charged acceptor nucleus. Importantly, from the thermally broadened single-electron transport through the localized acceptor state, in conjunction with the spectral shift of the valence band due to the ionized nucleus, the dopant depth can be directly correlated to its ionization energy.

The schematic energy diagrams in Fig. 1 illustrate three different transport regimes in which we study the sub-surface boron acceptors: (i) charge sensing in the valence band, (ii) resonant tunneling through the localized acceptor state and (iii) charge sensing in the conduction band. When a negative sample bias voltage is applied, the presence of a sub-surface acceptor results in an increase in the direct tunneling into the valence band

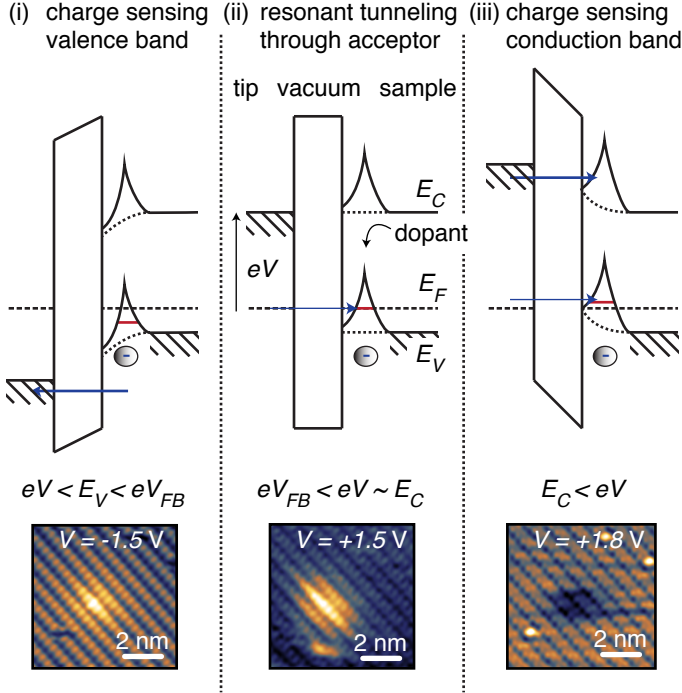


FIG. 1. Schematic energy diagram of the tip-vacuum-sample tunnel junction. (i) When $eV < E_V < eV_{FB}$ electrons tunnel from the valence band to the tip and the presence of a sub-surface acceptor is observed as a protrusion in the STM topography. (ii) In case $eV_{FB} < eV \sim E_C$ direct tunneling via the localized acceptor state leads to a protrusion in the topography. (iii) Suppression of the local density of states by the acceptor potential reduces the tunnel current when $E_C < eV$, resulting in a depression in the topography.

due to an increase in the local density of states (LDOS) caused by the negatively charged nucleus of the acceptor. The increase in tunnel current leads to a height increase in the STM topography, as is shown in figure 1(i). Likewise, when a positive voltage is applied, suppression of the local density of states by the acceptor potential leads to a decrease in the direct tunnel current into the conduction band and resulting in a dip in the STM topography [16](Fig. 1(iii)). However, when a positive voltage is applied such that the Fermi energy of the tip is close to the conduction band edge, the transport is no longer dominated by direct tunneling into the conduction band but by resonant transport through the localized acceptor state (Fig 1(ii)).

Since the Fermi energy of the heavily B-doped sample is pinned at the bulk acceptor level E_A^{bulk} , the voltage at which the localized acceptor state is equal to the Fermi level, V_{onset} , with respect to the flat-band voltage, V_{FB} , is a direct measure for the difference in ionization energy, $\Delta E = E_A - E_A^{bulk}$, of the sub-surface acceptor with respect to the bulk ionization energy. The bias dependence of the energy level of the localized acceptor state E_A is described by the lever arm $\alpha = e^{-1}dE_A/dV$ [18, 19]. In

this Letter we present a direct measurement of the lever arm and measure the shift $\Delta E = -\alpha e(V_{onset} - V_{FB})$ by studying transport through individual sub-surface acceptors where we directly determine: (i) the potential due to the negatively charged nucleus, (ii) the flat-band voltage and depth of the acceptors from direct tunneling to/from the conductance/valence band and (iii) the onset voltage and lever arm from single-electron transport through the localized acceptor state.

Figure 2(a) shows the normalised conductance $G_N = (dI/dV)/(\bar{I}/V)$ measured away from any sub-surface acceptor. The flat-band voltage V_{FB} was extracted by comparing the 4.2 K bandgap of Si(001):H with voltages V_V and V_C for tunneling into the valence and conduction band edges (dashed lines in Fig. 2(a) and (b)). A first approximation of V_{FB} is made by taking the tip induced band bending (TIBB) to be linear (dotted line in Fig. 2(b)). This constraint is subsequently relaxed in order to account for screening (solid line in Fig. 2(b)). Finally, the flat-band condition was independently measured from the apparent barrier height.

The onset voltage for tunneling from the valence band V_V and tunneling into the conduction band V_C is determined by finding the voltage axis intercept (i.e., $G_N = 0$) of the linear extrapolation of the $G_N - V$ curve at its maximum slope point (dotted lines in Fig. 2(a)) [20]. The potential $\phi_S(V)$ at the interface as a function of the applied sample voltages is obtained by from the flat-band energies $E_F - E_V = E_A^{bulk} - E_V = 0.045$ eV [21] and $E_g = E_C - E_V = 1.17$ eV at $T = 4.2$ K [22] away from the acceptor. Assuming a linear relationship between the applied voltage and the potential at the interface

$$\frac{d\phi_S}{dV} = \frac{e(V_C - V_V) - E_g}{V_C - V_V}, \quad (1)$$

yields an approximated flat-band voltage $V_{FB} = 0.5 \pm 0.1$ V which is inferred from the condition for tunneling from the valence band $\phi_S(V_V) = eV_V$

$$\frac{d\phi_S}{dV}(V_V - V_{FB}) = eV_V. \quad (2)$$

When the flat-band voltage lies within the band gap the $d\phi_S/dV$ can not be assumed linear as it is well known that for $V > V_{FB}$ accumulated carriers at the surface will screen the electric field from the tip more strongly. In order to correct for this effect we use the $\phi_S(V)$ calculated using the method of Feenstra [23] (Fig. 2(b)) and determine a corrected flat-band voltage $V_{FB} = 0.38 \pm 0.1$ V. This flat-band voltage is smaller than expected from the difference between the bulk workfunction $\Phi = 4.55$ eV [24] of tungsten and sample electron affinity $\chi = 4.05$ eV [25]. The measured flat-band voltage corresponds to a tip workfunction $\Phi_{tip} = 4.9 \pm 0.1$ eV (larger values for the tip workfunction have been previously reported). Finally, we independently confirmed the value of the tip

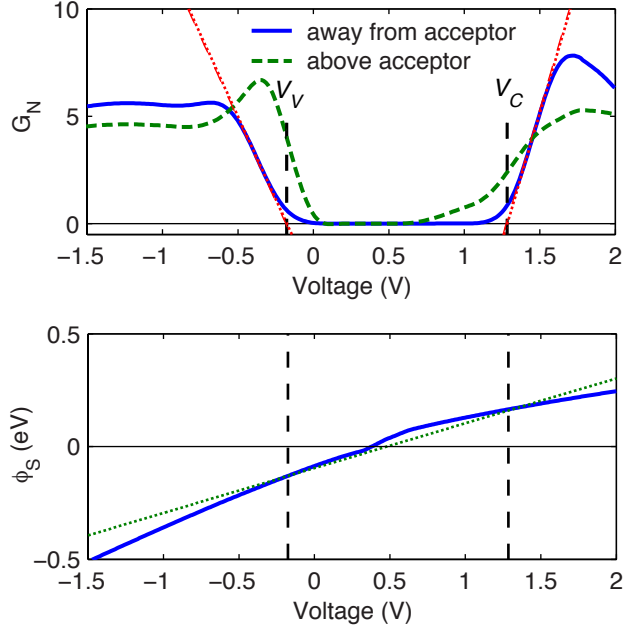


FIG. 2. (a) Normalized conductance G_N measured on a hydrogen terminated Si(100):H surface away from (solid line) and above (dashed line) an acceptor. The top of the valence band V_V and bottom of the conduction band V_C are determined by the slopes of G_N away from the acceptor (dotted lines). (b) Surface potential ϕ_S assuming linear TIBB (dotted line) and non-linear TIBB (solid line) calculated using the code developed by Feenstra [23].

workfunction by measuring the apparent barrier height [14, 26] (see section 1 of the Supplementary Material).

The distance of the sub-surface acceptors to the interface is measured from the spectral shift of the valence band edge. Figure 3(a) shows the differential conductance (dI/dV) map, as a function of position and sample bias voltage V , measured simultaneously with the empty state topography at $V = 2$ V shown in Fig. 3(a). At the acceptor site the dI/dV map clearly shows an upward spectral shift of the valence band states due to the buried acceptor. The spatially resolved shift of the valence-band edge ΔE_V as shown in Fig. 3(b) is defined from the slope of G_N as before. The first-order perturbation to the binding energy of the valence band states at the interface, ψ_s , and thus the shift of the valence-band edge, ΔE_V , due to the potential of the negatively charged acceptor nucleus at position r_0 can be estimated as

$$\Delta E_V = \langle \psi_s | U_A(r, r_0) | \psi_s \rangle, \quad (3)$$

where $U_A(r, r_0)$ is the acceptor potential at position r . In the case of a classical half-space, i.e. in the absence of screening by free carriers in the tip or the substrate, the approximation $\langle \psi_s | U_A(r, r_0) | \psi_s \rangle \approx U_A(s, r_0)$, where s is the lateral separation with respect to the acceptor

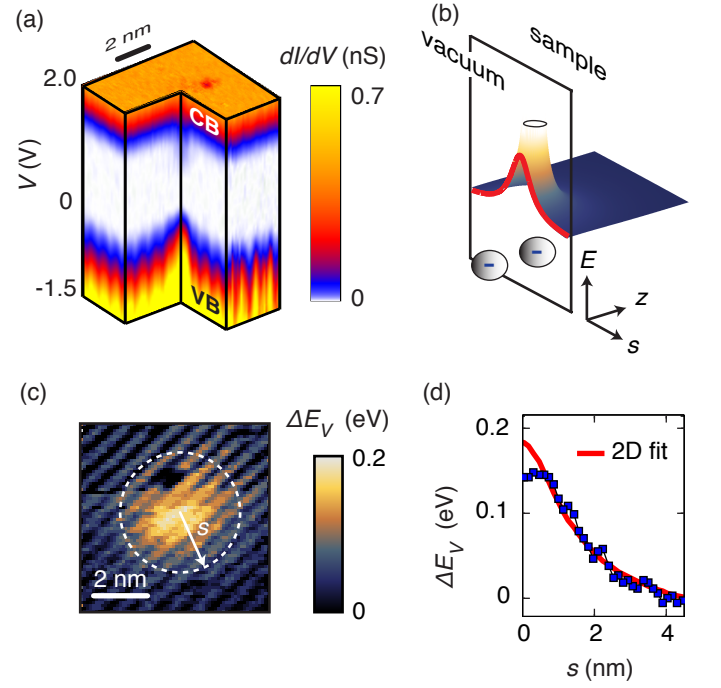


FIG. 3. (a) dI/dV map recorded simultaneously with empty-state topography (+2.2 V, 300 pA). Tunneling from the valence band to the tip is indicated by VB, tunneling from the tip to the conduction band is indicated by CB. The dI/dV map is cut at the acceptor site to show the upward shift of the valence band states. (b) Schematic potential landscape due to a negatively charged nucleus below the sample surface and its image charge in the vacuum. The solid line indicates the potential along the vacuum-semiconductor interface. (c) Shift in the valence band maximum E_V as function of lateral tip position. (d) Azimuthal averaged shift in the valence band maximum E_V (filled squares) as function lateral tip separation s from the acceptor as indicated in (c). The dopant depth is determined by fitting E_V to a bare Coulomb potential (solid line), taking into account the image charge due to dielectric mismatch as illustrated in (b).

nucleus along the interface as shown in Fig. 3(b), yields

$$\Delta E_V \approx \frac{e^2}{4\pi\epsilon_0\epsilon_{eff}} \frac{1}{\sqrt{s^2 + d^2}}, \quad (4)$$

where the modified dielectric constant ϵ_{eff} and depth d can be independently determine from a fit [15, 27]. The modified dielectric constant at the interface $\epsilon_{eff} = (\epsilon_v + \epsilon_{Si})/2$ is due to the mismatch between the dielectric constants ϵ_v and $\epsilon_{Si} = 11.4$ [28] of the vacuum and silicon, respectively, which leads to a single image charge at $-d$ as shown in Fig. 3(c). Figure 3(d) shows measured (filled squares) and fitted (solid line) spectral shift of the valence-band edge ΔE_V as function of lateral tip separation s from the dopant. Following references [15, 27] we fit the spectral shift of the valence-band edge as a function of position to equation 4 (Fig. 3(d)) and independently determine the depth d of individual

acceptors and the modified dielectric constant ϵ_{eff} . Importantly, any screening by either by carriers in the tip or in the substrate would reduce the effect of dielectric mismatch and thus lead to a deviation of the modified dielectric constant from $\epsilon_{eff} = (\epsilon_v + \epsilon_{Si})/2$. The obtained modified dielectric constant for all five measured acceptors agree within experimental error with the expected value $\epsilon_{eff} = 6$ following the classical half-space approach and experimental values that have previously been reported for STM experiments [15, 27].

We use the thermal broadening of the conductance peaks to calibrate the lever arm α for individual acceptors. The shift of the acceptor energy levels ΔE due to the applied bias voltage V depends on the screening of the electric field in the semiconductor and the overlap between the acceptor wavefunction and the TIBB (Fig. 4(a)). When screening is strong, the majority of the applied voltage will be dropped over the vacuum separating the tip and the sample and the potential in the semiconductor will only be slightly modified by the applied sample voltage. Furthermore, the lever arm will be smaller for acceptors deeper below the surface, as the electric field is more strongly screened further from the interface.

In previous studies the tip induced band bending has been estimated by solving the one- or three-dimensional Poisson equation [13, 19, 23, 26]. However, the calculated potential in the semiconductor will strongly depend on experimental parameters, e.g. tip-sample separation, tip shape and carrier concentration. Although in some cases these experimental parameters can be fitted from the data [19], they are typically not known. Moreover, the estimate of the lever arm from calculating the overlap between the TIBB and the impurity wavefunction is very sensitive to exact size of the wavefunction, which is well known to differ from the bulk wavefunction [18, 19]. Rather than trying to estimate the lever arm by solving the Poisson equation, we fit the conductance peak to a thermally broadened Lorentzian [29], as shown Fig. 4(b). This line shape describes resonant tunneling via a single localized state into a continuum of states that are occupied according to the Fermi-Dirac distribution [30, 31]. Other broadening mechanisms, e.g. lifetime broadening and charge noise, can be excluded as dominant sources of conductance peak broadening since they do not have the appropriate line shape of the conductance peaks and the fact that the width of the peaks does not increase with sampling time (see section 2 of the Supplementary Materials). By allowing α to vary linear with V in our fit we observe that the measured values for α do not depend on the bias voltage V . Consequently, we can conclude Stark shifts of the localized states due to the electric field is negligible in our measurement geometry. For consistency we compare our method with the previously described method [13, 19, 23, 26]. We have calculated V_{onset} and

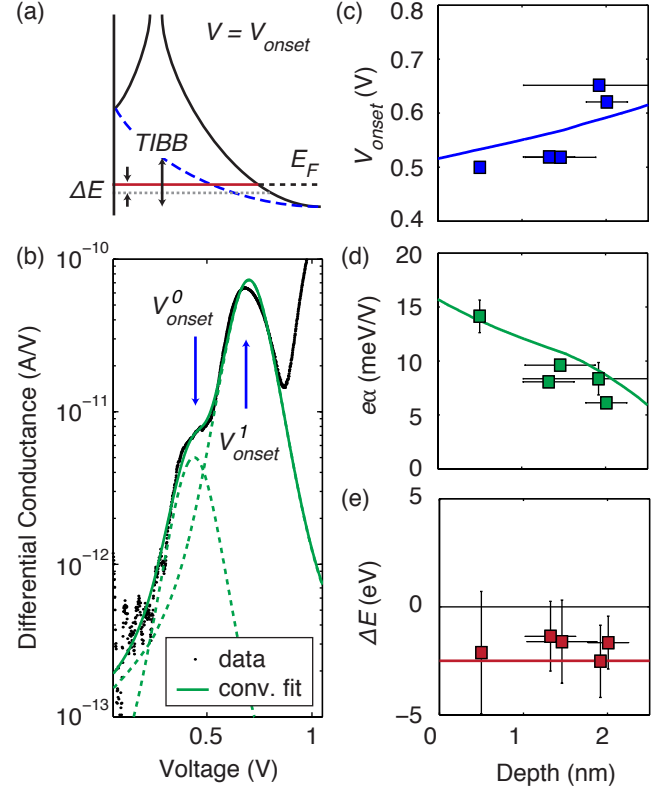


FIG. 4. (a) Schematic energy diagram. Local tip induced band bending brings the acceptor level E_A into resonance with the Fermi energy. The voltage V_{onset} at which this occurs depends on the acceptor depth, ionization energy and the screening length. (b) The lever arm α and the onset voltage V_{onset} are determined fitting the two conductance peaks in the bandgap to the sum of two thermally broadened Lorentzian line shapes. (c) Measured (squares) and calculated (line) onset voltage for resonant tunnelling as a function of acceptor depth. (d) Measured (squares) and calculated (line) lever arm as a function of acceptor depth. (e) The shift in ionization energy ΔE with respect to the bulk ionisation energy inferred from the measured onset voltage and the lever arm (squares). The onset voltage and lever arm are calculated for $\Delta E = -2.5$ meV, line in (c), and an overlap between the acceptor wavefunction and the tip induced band bending $\Delta E = -0.06 \times \text{TIBB}$, where TIBB is the tip induced band bending at the acceptor site as illustrated in (a).

α as a function of depth for $\Delta E = 2.5$ meV where we use the overlap between the impurity wavefunction and the TIBB as a free parameter to match the empirical result. We find that for $\Delta E = -0.06 \times \text{TIBB}$ the Poisson model matches our results. Importantly, the 0.06 overlap is a factor ~ 4 smaller the 0.27 overlap predicted in previous studies [13, 19]. The predicted uncertainty for the Poisson model is of the order of a factor 4 [13].

Figure 4(c) shows the onset voltage V_{onset} as a function of dopant depth for five different acceptors. The measured lever arm α is shown in Fig. 4(d). The shift in ionization energy $\Delta E = -\alpha e(V_{onset} - V_{FB})$

is smaller than zero for all measured acceptors, as shown in Fig. 4(e). Since the measured value of ϵ_{eff} corresponds to the expected value following the classical half-space approach we can conclude that two opposing effects influence the ionization energy of near-interface dopant atoms: (i) dielectric mismatch; the dopant potential, which is screened by charge polarization in the semiconductor, becomes more attractive when its environment becomes less polarizable, i.e. has a lower dielectric constant, which leads to an increase of the ionization energy; (ii) quantum confinement; exclusion of the dopant wavefunction from the region outside the semiconductor results in a decrease of the ionization energy [9, 10]. The observed bulk-like ionization energies for acceptors less than an effective Bohr radius from the interface are strong evidence that the effect of dielectric mismatch at the interface is mitigated by quantum confinement. Our transport data unambiguously demonstrates that acceptors within an effective Bohr radius from the interface of a silicon half-space geometry are not deactivated. We would like to point out that atomistic differences from the bulk may lead to an alteration of the binding energy such as the enhancement observed in the same geometry in Ref. [18], but this effect is unrelated to dielectric mismatch.

In conclusion, we have determined the ionization energy of individual sub-surface acceptors below the Si(100):H surface by means of low-temperature scanning tunneling spectroscopy. Calibration of the local lever arm using the thermal broadening of the conductance peaks removes the necessity of modeling the tip induced electrostatic potential below the semiconductor surface, providing a direct measure for the ionization energy. We believe that this method provides a valuable parallel between extensively studied electron transport in mesoscopic devices and scanning tunneling spectroscopy. Moreover, this experiment demonstrates bulk-like ionization energies for acceptors less than a Bohr radius away from the interface. The fact that sub-surface acceptors are not deactivated is of great importance for the doping of nanoscale devices.

This research was conducted by the Australian Research Council Centre of Excellence for Quantum Computation and Communication Technology (project number CE110001027) and the US National Security Agency and the US Army Research Office under contract number W911NF-08-1-0527. M.Y.S. acknowledges an ARC Federation Fellowship. S.R acknowledges an ARC Future Fellowship.

[1] M. F. Bukhori, S. Roy, and A. Asenov, IEEE Transactions On Electron Devices **57**, 795 (2010).

[2] M. T. Björk, H. Schmid, J. Knoch, H. Riel, and W. Riess, Nature Nanotechnology **4**, 103 (2009).

[3] M. Pierre, R. Wacquez, X. Jehl, M. Sanquer, M. Vinet, and O. Cueto, Nature Nanotechnology **5**, 133 (2009).

[4] M. Diarra, Y.-M. Niquet, C. Delerue, and G. Allan, Physical Review B **75**, 045301 (2007).

[5] H. Sellier, G.P. Lansbergen, J. Caro, S. Rogge, N. Collaert, I. Ferain, M. Jurczak, and S. Biesemans, Physical Review Letters **97**, 206805 (2006).

[6] J. Luttinger and W. Kohn, Physical Review **97**, 869 (1955).

[7] R. Loudon, American Journal of Physics **27**, 649 (1959).

[8] G.W. Bryant, Physical Review B **29**, 6632 (1984).

[9] Y.L. Hao, A.P. Djotyan, A.A. Avetisyan, and F.M. Peeters, Physical Review B **80**, 035329 (2009).

[10] M.J. Calderon, J. Verduijn, G.P. Lansbergen, G.C. Tetamanzi, S. Rogge, and B. Koiller, Physical Review B **82**, 075317 (2010).

[11] A. M. Yakunin, A. Y. Silov, P. M. Koenraad, J.-M. Tang, M. E. Flatte, J. L. Primus, W. van Roy, J. de Boeck, A. M. Monakhov, K. S. Romanov, I. E. Panaiotti, and N. S. Averkiev, Nature Materials **6**, 512 (2007).

[12] S. Loth, M. Wenderoth, and R.G. Ulbrich, Physical Review B **77**, 115344 (2008).

[13] J.K. Garleff, A.P. Wijnheijmer, A.Y. Silov, J. van Bree, W. VanRoy, J.M. Tang, M.E. Flatte, and P.M. Koenraad, Physical Review B **82**, 035303 (2010).

[14] A. P. Wijnheijmer, J. K. Garleff, M. A. von d Heijden, and P. M. Koenraad, Journal Of Vacuum Science & Technology B **28**, 1086 (2010).

[15] D. H. Lee and J. A. Gupta, Science **330**, 1807 (2010).

[16] F. Marcinowski, J. Wiebe, J.-M. Tang, M.E. Flatte, F. Meier, M. Morgenstern, and R. Wiesendanger, Physical Review Letters **99**, 157202 (2007).

[17] H. Zheng, J. Kröger, and R. Berndt, Physical Review Letters **108**, 076801 (2012).

[18] A. P. Wijnheijmer, J. K. Garleff, K. Teichmann, M. Wenderoth, S. Loth, R. G. Ulbrich, P. A. Maksym, M. Roy, and P. M. Koenraad, Physical Review Letters **102**, 166101 (2009).

[19] A.P. Wijnheijmer, J.K. Garleff, K. Teichmann, M. Wenderoth, S. Loth, and P.M. Koenraad, Physical Review B **84**, 125310 (2011).

[20] R.M. Feenstra, Physical Review B **50**, 4561 (1994).

[21] A. Ramdas and S. Rodriguez, Reports on Progress in Physics **44**, 1297 (1981).

[22] C. Kittel, *Introduction to Solid State Physics* (John Wiley & Sons, 2004).

[23] R. Feenstra, Journal Of Vacuum Science & Technology B **21**, 2080 (2003).

[24] B. J. Hopkins and J. C. Rivière, Proceedings of the Physical Society **81**, 590 (2002).

[25] S. M. Sze and K. K. Ng, *Physics of Semiconductor Devices* (John Wiley & Sons, 2006).

[26] S. Loth, M. Wenderoth, R.G. Ulbrich, S. Malzer, and G.H. Dohler, Physical Review B **76**, 235318 (2007).

[27] K. Teichmann, M. Wenderoth, S. Loth, R. G. Ulbrich, J. K. Garleff, A. P. Wijnheijmer, and P. M. Koenraad, Physical Review Letters **101**, 076103 (2008).

[28] O. Madelung, *Semiconductors: Data Handbook* (Springer, 2004).

[29] E.B. Foxman, P.L. McEuen, U. Meirav, N.S. Wingreen, Y. Meir, P.A. Belk, N.R. Belk, M.A. Kastner, and S.J. Wind, Physical Review B **47**, 10020 (1993).

- [30] C.W.J. Beenakker, Physical Review B **44**, 1646 (1991).
- [31] D.V. Averin, A.N. Korotkov, and K.K. Likharev, Physical Review B **44**, 6199 (1991).